Vibrational spectroscopic studies of aqueous solutions of *tert*-butyl alcohol and *tert*-butylamine

Pius K. Kipkemboi and Allan J. Easteal

Abstract: Raman and FT-IR absorption spectra of aqueous *tert*-butyl alcohol (*t*-BuOH) and *tert*-butylamine (*t*-$BuNH_2$) in the region of the O–H and NH_2 stretching and bending modes have been measured as a function of organic co-solvent concentration in the whole co-solvent mole fraction region. The major observed changes of the aqueous binary solution spectra compared with the solvent spectra are a loss or gain of band intensity. In particular, the observed changes in intensities and linewidths of some bands were significantly more pronounced at low concentrations of organic co-solvents in water, where *t*-BuOH and *t*-$BuNH_2$ tend to integrate into the water structure. Clear evidence of structural enhancement of the network is obtained in dilute solutions as well as destruction of the network by hydrophobic interactions as the concentration is increased. Generally, the interpretation of the spectra is in agreement with the capacity of the hydrophobic co-solvent to break the structure of water in the more concentrated aqueous solutions and to enhance the structure in dilute solutions. Vibrational intensities and frequency shifts of some bands show definite trends with varying the concentration of the solutions. In the concentration-dependence study, unusual linewidth changes of certain bands were observed.

Key words: infrared, Raman spectra, aqueous, *tert*-butanol, *tert*-butylamine.

Résumé : On a mesuré les spectres d'absorption Raman et infrarouges en transformée de Fourier de solutions aqueuses de *tert*-butanol (*t*-BuOH) et de *tert*-butylamine (*t*-$BuNH_2$), dans la région des modes d'élongation et de déformation du O–H et du NH_2, en fonction de la concentration du cosolvant organique, sur toute la plage des fractions molaires du cosolvant. Les changements principaux observés dans les spectres en solutions aqueuses binaires par rapport à ceux des spectres du solvant sont des gains ou des pertes dans l'intensité de la bande. En particulier, les changements observés dans les intensités et les largeurs de quelques bandes sont beaucoup plus prononcés à de faibles concentrations des cosolvants organiques dans l'eau vers laquelle le *t*-BuOH et la *t*-$BuNH_2$ ont tendance de migrer dans la structure de l'eau. On a obtenu des données claires en faveur d'une augmentation de la structure du réseau en solutions diluées ainsi que de la destruction du réseau par les interactions hydrophobes avec une augmentation de la concentration. En général, l'interprétation des spectres est en accord avec la capacité du cosolvant hydrophobe à briser la structure de l'eau dans les solutions aqueuses plus concentrées et à les augmenter en solutions diluées. Les intensités vibrationnelles et les déplacements dans les fréquences de quelques bandes présentent des tendances bien définies avec les variations dans les concentrations dans les solutions. Dans l'étude sur la dépendance sur la concentration, on a observé des changements inhabituels dans la largeur de certaines bandes.

Mots clés : infrarouge, spectre Raman, aqueux, *tert*-butanol, *tert*-butylamine.

[Traduit par la Rédaction]

Introduction

Vibration spectra are, in general, sensitive to the local environment of a molecule, and information concerning the relative position of the molecule in quite a short time can be obtained from the spectra. Vibrational spectra of water or aqueous solutions have received considerable attention in relation to the liquid structure of water. Although numerous papers have been presented reporting spectra of inorganic electrolytes in aqueous solution, there are few studies on the vibrational spectra of organic molecules in water (1–10). It is of interest to interpret vibrational spectra of organic molecules in aqueous solution and to discuss the intermolecular interactions and liquid structures in the these systems.

In the present investigation, FT-IR and Raman spectra of aqueous *tert*-butanol and *tert*-butylamine in the O–H stretching and bending regions were measured at room temperature as a function of co-solvent concentration in the entire co-solvent mole fraction region. The purpose of this study was to investigate the structural changes brought about by a change in the concentration of co-solvent. It was anticipated that FT-IR and Raman spectroscopy of aqueous solutions of the aforementioned compounds would provide insights into the structural perturbations of bulk water, which are caused by hydrophobic co-solvents, and provide a structure-oriented conceptual framework for evaluating various hydrophobic effects. In the present study, the two co-solvents, *tert*-butyl alcohol (*t*-BuOH) and *tert*-butylamine (*t*-$BuNH_2$), were used

Received 14 December 2001. Published on the NRC Research Press Web site at http://canjchem.nrc.ca on 20 June 2002.

P.K. Kipkemboi.[1] Department of Chemistry, Moi University, P.O. Box 1125, Eldoret, Kenya,
A.J. Easteal. Department of Chemistry, The University of Auckland, Private Bag 92019, Auckland, New Zealand.

[1]Corresponding author (e-mail: keronei@yahoo.com).

 DOI: 10.1139/V02-102

because they are relatively hydrophobic yet completely miscible with water in all proportions. H_2O + *t*-BuOH and H_2O + *t*-$BuNH_2$ mixtures provide a useful opportunity for investigating the interactions of a non-electrolyte with water. Both *t*-BuOH and *t*-$BuNH_2$ hydrophobic co-solvents may serve as model compounds for more complicated aqueous systems like surfactants, emulsions, and biopolymers.

Most of the essential functions of macromolecules in living materials are determined by the hydrogen-bonded structures. The vibrational modes of NH- and OH-stretch character, therefore, carry valuable function-related structural information. Since life is inseparably connected with the presence of water, water as a solvent should be used to study biological molecules (3). Overlap of the vibrational bands of water with those of solutes is inevitable, resulting in broadband contours, which cannot usually be deconvoluted into their constituents (11, 12). In this study, we explored the fact that vibrational spectra of solvent water are very sensitive to the nature of solute. Network-perturbing hydrophobic organic co-solvents can provide useful information about aqueous solutions of non-electrolytes, but the interpretation is complicated by the different stretching frequencies for N–H···O bonds compared with O–H···O bonds.

Our previous work focussed on investigating the thermodynamic and mass transport behaviour of such systems (13–17). Studies of aqueous solutions of *t*-BuOH and *t*-$BuNH_2$ showed an "enhancement" of the water structure by the co-solvent (*t*-BuOH or *t*-$BuNH_2$) at very low concentrations. In contrast, at higher concentrations, both co-solvents disrupt the structure of the water, behaving as "structure breakers." In this work such previous data are extended and consolidated with Raman and FT-IR spectra. Although the vibrational spectra of the H_2O + *t*-BuOH system were previously reported (5), there are few data available for the H_2O + *t*-$BuNH_2$ system.

Experimental

Materials

tert-Butyl alcohol was supplied by Riedel-de Haën and *tert*-butylamine by Aldrich. The stated purity of both solvents exceeded 99.0 mol%. The solvents were dried using thermally activated molecular sieves (3 Å). Ultra-pure water from a milli-Q purification system was used.

Binary mixtures were prepared by weighing appropriate amounts of the components into fine glass vials using a balance with accuracy ±0.1 mg.

Apparatus and procedures

Raman spectra were recorded with a Jobin-Yvon V1000 spectrometer, a double monochromator instrument equipped with holographic gratings (1600 grooves per mm) for high resolution and good stray-light rejection. A Spectra-Physics Model 2016 argon ion laser was used as the excitation source and non-lasing plasma lines were removed with a Laser III premonochromator. The filtered laser light was diverted to the macro sampling chamber using a flip mirror. The Raman scattered radiation was detected with a gallium–arsenide photomultiplier tube (PMT), which was cooled by a Peltier-effect device to ca. 250 K to reduce the thermal noise. A spectralink module, connected to the PMT and interfaced to an IBM PC-compatible computer, provided photon counting, data acquisition, and monochromator drive. Liquid samples in glass vials were attached to a motor drive unit situated in the macrochamber of the spectrometer. The vial was then spun to enhance the Raman signal and to reduce the risk of sample decomposition. Typically 40–100 mW of focused-laser light was used. The Jobin-Yvon Prism software package was employed to operate the spectrometer. All data manipulations and spectral plottings were performed with Spectra Calc (Galactic Industries Corp.) software. The spectrometer was calibrated using the 514.5 nm line of the argon ion laser, and the spectra were reproducible to ±1 cm^{-1}. The spectra were obtained at a spectral resolution of 5 cm^{-1}, the data being collected at 2 cm^{-1} intervals. The scanning speed of the spectrometer was 1.0 cm^{-1} s^{-1} and the integration time was 0.5 s per data point. The acquisition time was 30 min. The spectral range covered was 4000–400 cm^{-1}. All the Raman spectra were recorded with the samples at room temperature.

Mid-IR spectra were recorded on a Digilab FTS-60 Fourier transform infrared spectrometer employing a Globar source, a KBr beam splitter, and an uncooled DTGS detector. The spectrometer was interfaced to a computer and a 68020 processor with Digilab software. The main body of the spectrometer was purged with dry nitrogen. Samples were examined as thin films using an attenuated internal

Fig. 1. Raman spectra of water, *t*-BuOH, and two *t*-BuOH aqueous solutions in the frequency range of 400–4000 cm^{-1}; mol% of *t*-BuOH are noted on each curve. Spectra are plotted as recorded but shifted in a vertical direction.

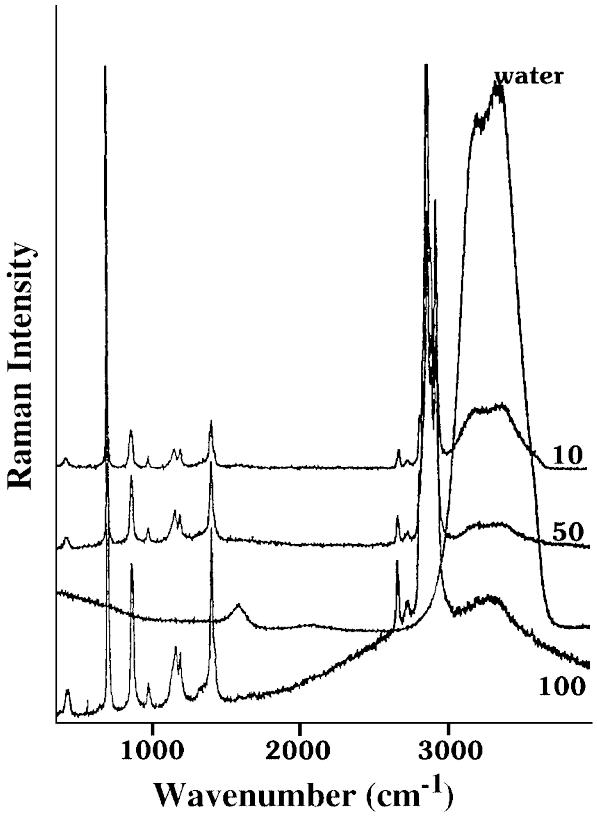

Fig. 2. Raman spectra as a function of composition for H_2O + *t*-BuOH mixtures in the region 2700–3800 cm^{-1}; mol% of *t*-BuOH are noted on each curve. Spectra are plotted as recorded but shifted in a vertical direction.

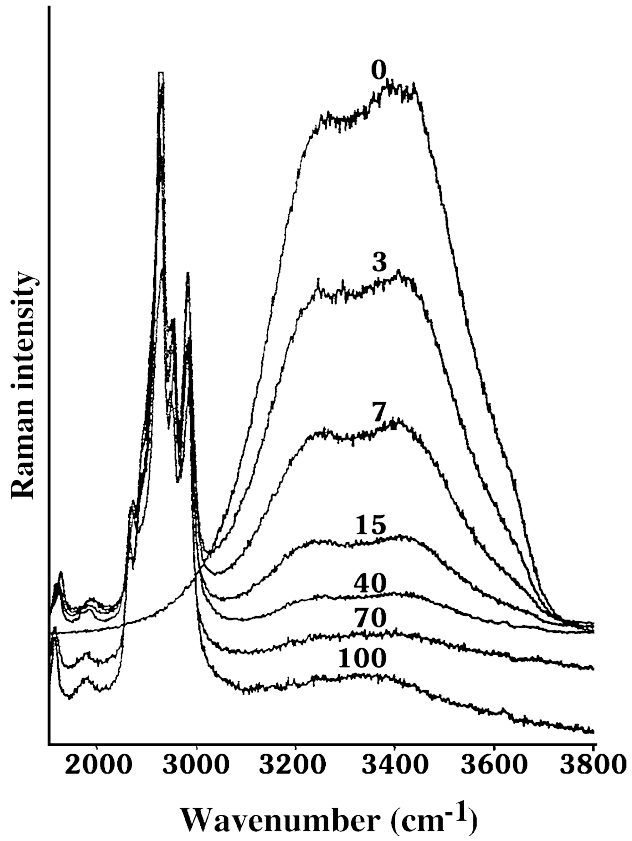

Fig. 3. IR spectra of H_2O + *t*-BuOH mixtures as a function of composition in the region 2800–3600 cm^{-1}; mol% of *t*-BuOH are noted on each curve. Spectra are plotted as recorded but shifted in a vertical direction.

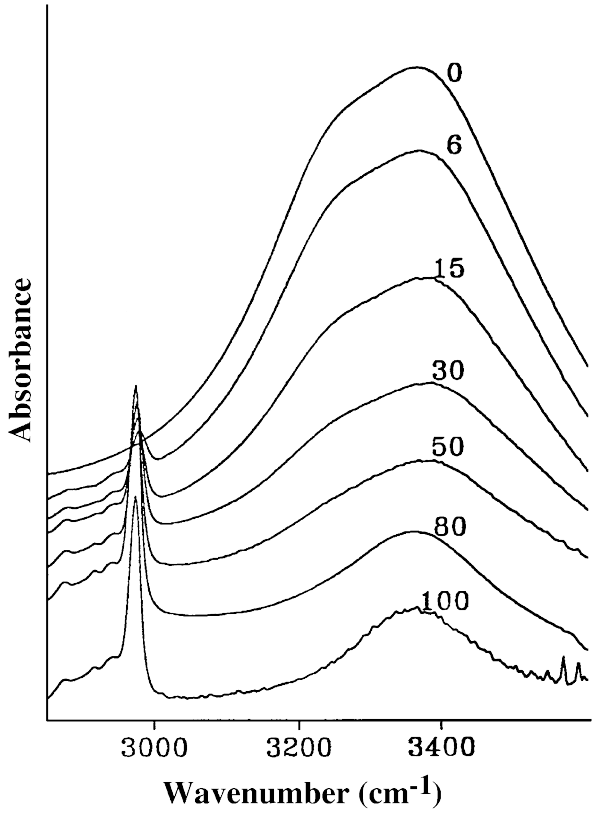

reflectance (ATR) accessory. Internal reflection spectroscopy was performed using multiple-reflection ATR parallelogram with a 45° angle of reflection. A clean dry Silicon ATR element was used to obtain a single-beam background spectrum. The ATR cell was then filled with a sample solution using syringe pressure and scanned to obtain absorbance spectra. The sample in the ATR cell was purged for at least 5 min with nitrogen gas before spectra were recorded. Between sample runs, the cell was flushed with water and acetone and then dried with ambient air. Thirty interferograms were collected, co-added, apodized with a triangular function, and Fourier transformed to give spectra of 4 cm^{-1} resolution. Spectral manipulations were performed with Spectra Calc. All spectra reported here were obtained using a Silicon ATR cell at room temperature. The spectral range covered was 4000–1050 cm^{-1}.

Results and discussion

Vibrational spectra of H_2O + *t*-BuOH mixtures

Figure 1 represents the Raman spectra of water, *t*-BuOH, and two *t*-BuOH solutions of different concentrations recorded in the frequency range of 400–4000 cm^{-1}. In Fig. 2, the Raman spectra of various H_2O + *t*-BuOH mixtures in the 2700–3800 cm^{-1} region are shown in more detail and compared with the spectrum of water. These spectra were recorded with the same incident-laser power and no further corrections, such as for refractive index, were made. Figure 2 allows us to follow the effect of *t*-BuOH concentration on the water organization. The broad feature dominating the spectrum is due to the O–H stretching mode of water. The strongest Raman band observed for liquid *t*-BuOH is polarized and found at ~752 cm^{-1}. This band is attributed to the in-phase C_3C–O stretching mode. A CH_3 stretching band for *t*-BuOH appears in the 2800–3000-cm^{-1} region and is clearly seen even in systems with high water content. In pure liquid *t*-BuOH only one broad O–H stretching vibration band appears in the high-frequency region centred around 3360 cm^{-1}, which has an antisymmetric contour. The band is very strong in the IR spectrum but very weak in the Raman spectrum. The small shoulder observed at ~3600 cm^{-1} in pure water seems to disappear as the concentration of *t*-BuOH increases. Nevertheless, it is difficult to determine if this apparent disappearance is due to the reduction in the intensity of this band or to the overlapping of the adjacent strong band. Needless to say, *t*-BuOH as well as *t*-$BuNH_2$ are not unique in this respect. For instance, hydrogen peroxide also suppresses the high-frequency shoulder in water (18). Electrolytes are also known to suppress the high-frequency shoulder in water (19).

In contrast, the position and shape of the O–H stretching vibrations of the two bands centred at ~3250 and 3400 cm^{-1} remain almost constant with an increase in the concentration

Fig. 4. IR spectra of H_2O + *t*-BuOH mixtures as a function of composition in the region 1100–1750 cm^{-1}; mol% of BuOH are noted on each curve. Spectra are plotted as recorded but shifted in a vertical direction.

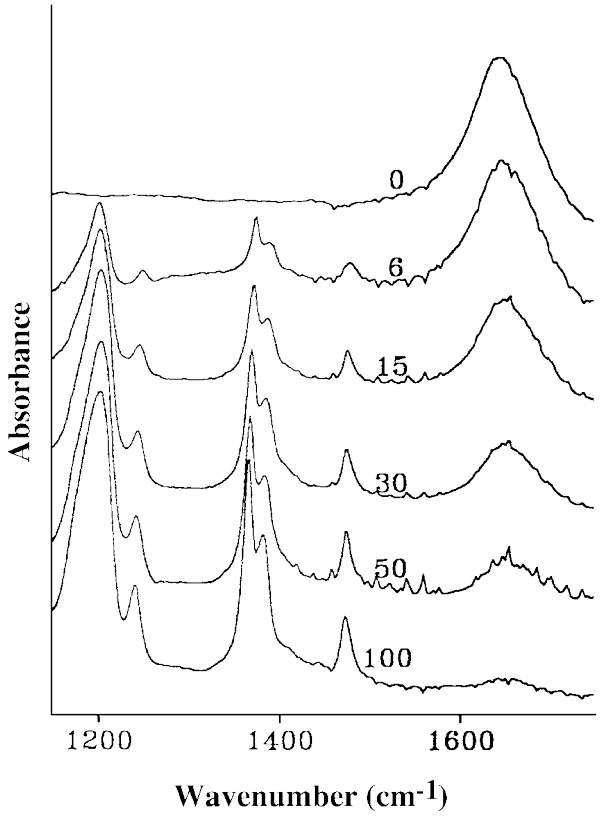

Fig. 5. Raman spectra of water, *t*-$BuNH_2$, and two *t*-$BuNH_2$ aqueous solutions in the frequency range of 400–4000 cm^{-1}; mol% of *t*-$BuNH_2$ are noted on each curve. Spectra are plotted as recorded but shifted in a vertical direction.

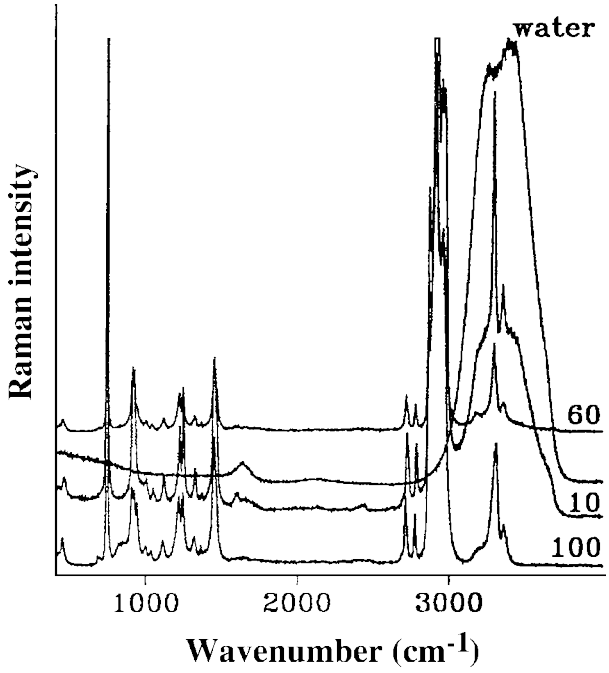

of *t*-BuOH. At low concentrations (≤15 mol% *t*-BuOH), however a sharp decrease in the intensity of the O–H stretching mode of water is observed. Thus, Figs. 1 and 2 show that the primary effect of the addition of *t*-BuOH is the reduction in the intensity of the two bands. The decrease in intensity of the two peaks at moderately high concentrations of *t*-BuOH (i.e., >15 mol%) is less noticeable indicating that the network structure of bulk water has been significantly disrupted at these concentrations.

The IR spectra of several H_2O + *t*-BuOH systems with increasing mole fractions of *t*-BuOH are presented in Fig. 3. The position of the low-frequency shoulder at ~3250 cm^{-1} remains relatively constant. It can be seen, however, that the prominence of the low-frequency shoulder continuously decreases with increasing *t*-BuOH content and eventually vanishes at high concentrations. It is difficult to follow the absorption profile of the high-frequency broad band centred at ~3400 cm^{-1} of water because it occurs in the same region as the strong broad absorption band of *t*-BuOH. It is noteworthy that the peak shows a frequency shift towards higher wavenumbers with increasing concentration of *t*-BuOH, at least up to 50 mol% co-solvent.

With the exception of the water bending mode at 1650 cm^{-1}, there were no significant changes in the Raman or IR spectra of the H_2O–*t*-BuOH system in the region below 2800 cm^{-1} with change in composition. But, as shown in Figs. 1 and 4, the intensity of the vibrational bending mode of water in both Raman and IR decreases considerably with increasing *t*-BuOH concentration until it vanishes at high concentrations, but its position seems to be invariant.

Vibrational spectra of H_2O + *t*-$BuNH_2$ mixtures

Figure 5 represents the Raman spectra of water, *t*-$BuNH_2$, and two solutions of *t*-$BuNH_2$ in water recorded in the frequency range of 400–4000 cm^{-1}. These spectra were recorded with the same incident-laser power and no further corrections, such as for refractive index, were made. The strongest Raman band observed for *t*-$BuNH_2$ is polarized and found at ~750 cm^{-1}. This band is attributed to the symmetric C_3C–N stretching mode. The CH_3 stretching bands of *t*-$BuNH_2$ appear in the 2800–3000 cm^{-1} region and are clearly seen even in systems with high water content. The vibrational spectrum of pure liquid *t*-$BuNH_2$ contains two peaks between 3200 and 3400 cm^{-1}. In this region of the Raman spectrum, the strongest band at 3310 cm^{-1} is polarized and it is assigned to the symmetric NH_2 stretching mode, while the weak depolarized band at 3360 cm^{-1} is assigned to the corresponding antisymmetric stretching mode. In the IR spectrum, the band at 3360 cm^{-1} is fairly strong, whereas the peak at 3310 cm^{-1} is very weak. Figure 6 shows in more detail the variations in the Raman-band profiles of the NH_2 stretching modes as a function of the concentration of *t*-$BuNH_2$ in water. The high-frequency band at ~3360 cm^{-1} attributed to the NH_2 antisymmetric stretch is generally weak and very broad, making it difficult to follow its variation in intensity with composition. Our interest is therefore directed toward the much stronger NH_2 symmetric peak at 3310 cm^{-1}.

The low-frequency band centred at ~3310 cm^{-1} exhibits a frequency shift to higher wavenumbers with increasing concentration of *t*-$BuNH_2$ and its intensity changes in a

Fig. 6. Raman spectra for H_2O + *t*-$BuNH_2$ mixtures as a function of composition in the region 2700–3700 cm^{-1}; mol% of *t*-$BuNH_2$ are noted on each curve. Spectra are plotted as recorded but shifted in a vertical direction.

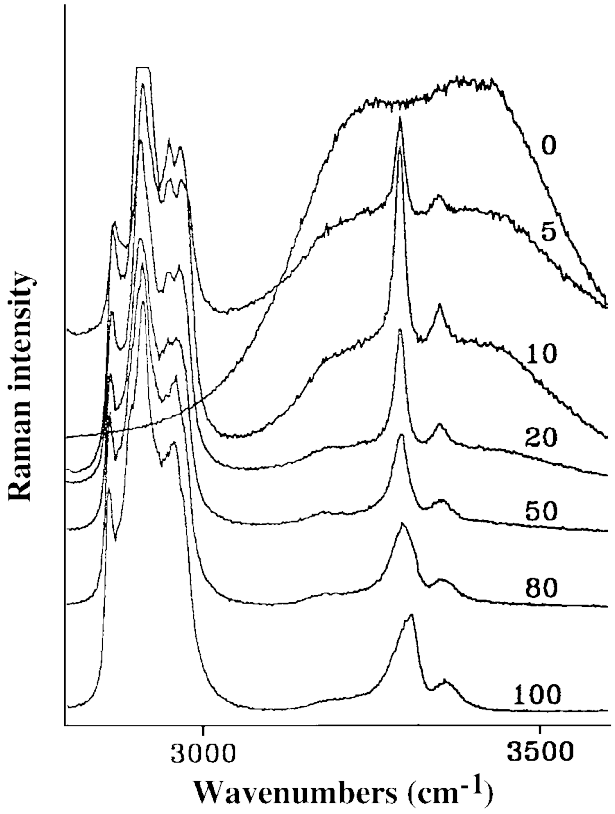

peculiar manner. As observed in Figs. 5 and 6, the intensity of the band seems to increase sharply as the concentration of *t*-$BuNH_2$ rises, passing through a maximum value in the water-rich region, and then shows a decreasing trend. To quantitatively follow the apparent change in peak intensity as a function of composition, the peaks were integrated. The CH_3 symmetric band at 2920 cm^{-1} was chosen as the reference band as it is very strong in Raman and its intensity does not seem to change significantly with the variation in the concentration of water, and furthermore, it is close to the band of interest. The band maxima of the NH_2 and CH_3 symmetric stretching vibrations were baseline corrected, and integration of the spectral profiles of their areas were determined using the Spectra Calc software. In Fig. 7, the variation of the integrated Raman intensity ratio ($I[3296cm^{-1}]_{NH_2}/I[2920cm^{-1}]_{CH_3}$) with composition is presented, where the peaks at 3296 and 2920 cm^{-1} are baseline corrected and the integrated intensity of the NH_2 and CH_3 components are measured. The concentration dependence of the integrated Raman intensity ratio is unique and characteristic. The ratio of integrated Raman intensity of the bands at 3296 and 2920 cm^{-1} as a function of *t*-$BuNH_2$ content is in qualitative agreement with previous results obtained with other techniques (13–16) — the intensity ratio shows a maximum around 10 mol% of *t*-$BuNH_2$. This demonstrates that *t*-$BuNH_2$ exhibits a strong hydrophobic hydration at low mole fractions, and that this hydration structure is broken down at higher mole fractions. We have followed the effect

Fig. 7. Ratio of Raman integrated intensity of the bands around 3296 and 2920 cm^{-1} as a function of composition.

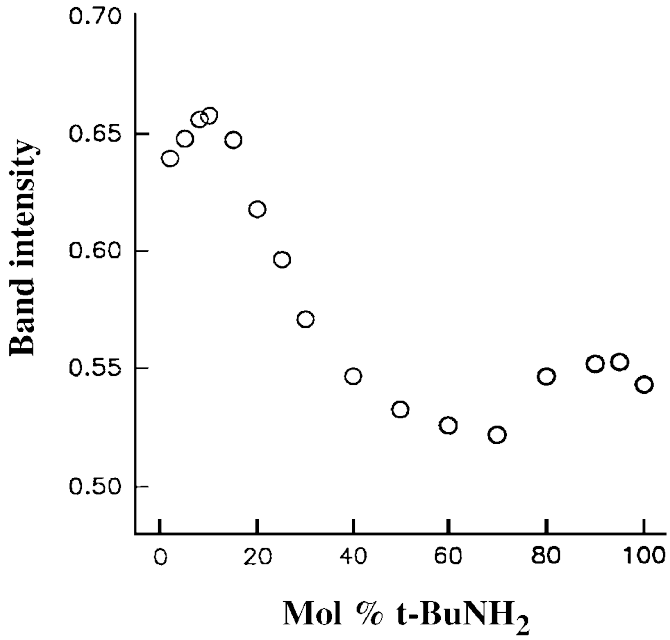

Table 1. Observed frequency and line width at half-maximum (FWHM) of the NH_2 symmetric stretch in the Raman spectra of *t*-$BuNH_2$ mixtures as a function of composition.

mol% *t*-$BuNH_2$	Frequency (cm^{-1})	FWHM (cm^{-1})
5.0	3294	17.3
10.0	3294	18.1
15.0	3294	18.2
20.0	3294	18.2
25.0	3296	21.8
30.0	3296	25.5
40.0	3296	26.4
50.0	3296	31.4
60.0	3296	34.9
70.0	3296	40.0
80.0	3298	44.5
90.0	3300	49.1
95.0	3305	50.5
100	3310	52.3

of concentration on the full width at half-maximum (FWHM) of the NH_2 symmetric stretching band at ~3296 cm^{-1}. The variation in apparent frequency shifts and line widths at half-maximum with concentration are presented in Table 1. As seen in Table 1, the line width at half-maximum below 20 mol% *t*-$BuNH_2$ does not depend on the concentration in water-rich solutions, being nearly constant in the water-rich region, but the dependence is remarkable above this concentration, showing a continuous and virtually linear change of line width from 18.2 to 52.3 cm^{-1} on going from 20 to 100 mol% *t*-$BuNH_2$.

It can be assumed that in the water-rich region (presumably below 15 mol% *t*-$BuNH_2$), the structure of the solution corresponds to the structure of pure water and the amine

Fig. 8. IR spectra of H_2O + t-$BuNH_2$ mixtures as a function of composition in the region 2600–4000 cm^{-1}; mol% of t-$BuNH_2$ are noted on each curve. Spectra are plotted as recorded but shifted in a vertical direction.

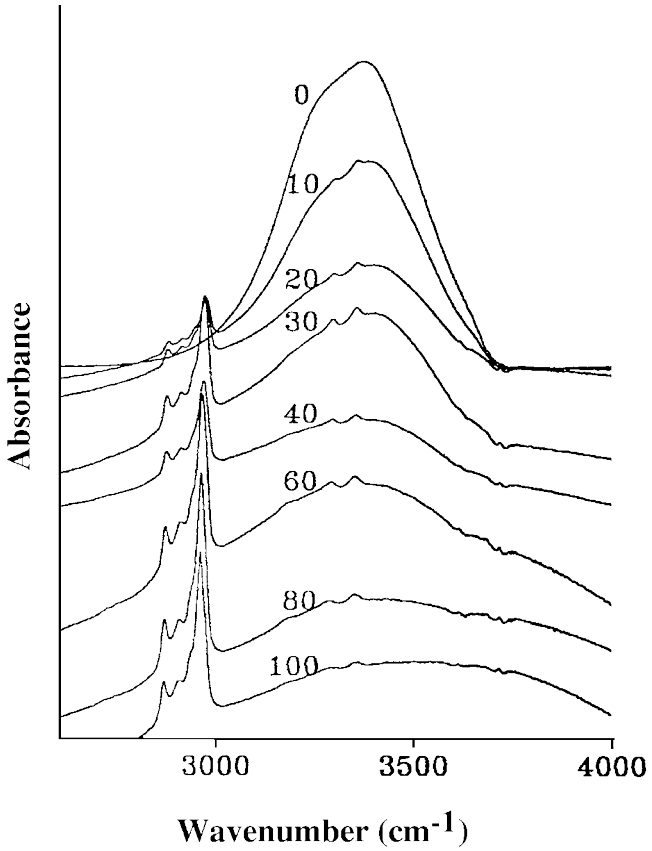

Fig. 9. IR spectra of H_2O + t-$BuNH_2$ mixtures as a function of composition in the region 1150–1750 cm^{-1}; mol% of t-$BuNH_2$ are noted on each curve. Spectra are plotted as recorded but shifted in a vertical direction.

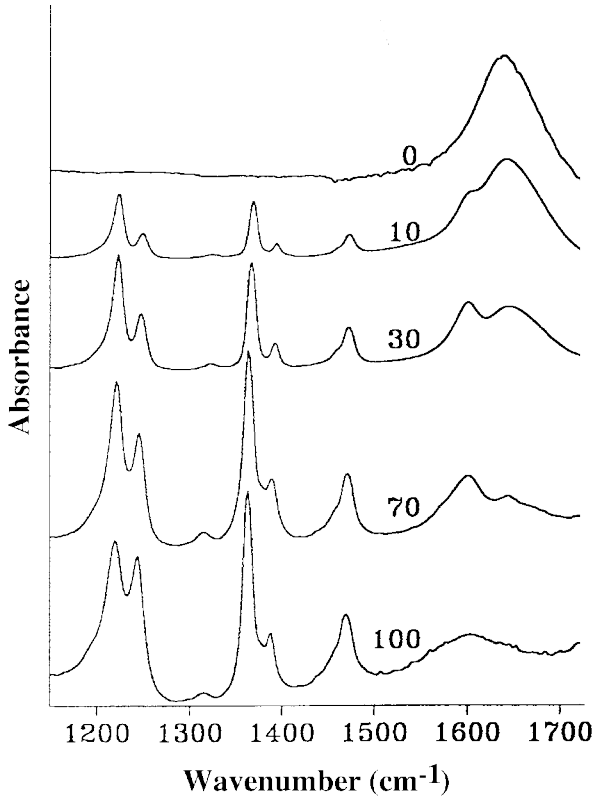

molecules are incorporated into the network structure of bulk water by cavity filling, thereby enhancing the water structure because of water–co-solvent hydrophobic interactions. But at higher concentrations of co-solvent the enhanced structure of water is gradually broken down by the organic co-solvent as the t-$BuNH_2$ molecules form hydrogen-bonds with water molecules. The formation of such hydrogen bonds between t-$BuNH_2$ and water gives rise to large line widths, similar to those in neat liquid t-$BuNH_2$. At relatively higher concentration of t-$BuNH_2$, the hydrogen bonds between t-$BuNH_2$ molecules are dominant — the more hydrogen-bonded the t-$BuNH_2$ molecules become the larger the observed line widths.

Good IR spectra of aqueous solutions of t-$BuNH_2$ were difficult to obtain due to the broad, intense water absorption bands, which obscure much of the mid-IR spectrum (the NH_2 stretching vibrations of t-$BuNH_2$, which are comparatively weak, occur in the same region). The O–H stretching region from 3100 to 3500 cm^{-1} is essentially opaque in the highly water-rich solvent (<10 mol% t-$BuNH_2$), and hence, the weak NH_2 stretching vibrations are completely masked.

As the concentration increases above 10 mol% t-$BuNH_2$, the broad O–H profile-band contour observed for water decreases gradually in intensity and the NH_2 stretching bands become more noticeable with no apparent shifts in their band positions. The band corresponding to the symmetric NH_2 stretching mode of t-$BuNH_2$, is a fairly intense band in Raman, but is much weaker in IR in comparison with the high-frequency band at ~3360 cm^{-1} attributed to the characteristic antisymmetric NH_2 stretching vibration. Changes in the relative intensities of these two bands were found to parallel the Raman intensity of the low-frequency component at ~3296 cm^{-1} (Figs. 6 and 7), since they seem to initially increase passing through maxima before apparently decreasing again with increasing concentration of t-$BuNH_2$. In Fig. 8, the variation in IR-band profiles of the OH and NH_2 stretching modes are shown as a function of concentration of t-$BuNH_2$ in water.

The bands at ~1645 and 1600 cm^{-1}, which are weak in the Raman but fairly strong in the IR, correspond to the bending vibrations of water and the NH_2 component of t-$BuNH_2$, respectively. The two bands are very sensitive to concentration. It is noteworthy that the peak absorbancies of the two bands vary in a nearly linear fashion with concentration, and can be used for analytical purposes. The trends of their absorbancies with concentration are shown in Fig. 9. It can be seen that the absorbance of the bending mode of water at ~1645 cm^{-1} decreases with the addition of t-$BuNH_2$ to water. The NH_2 bending mode initially appears as a shoulder at low concentrations of t-$BuNH_2$. As the mole fraction of t-$BuNH_2$ increases, this shoulder develops into a band centred at ~1600 cm^{-1}. Finally, the 1600 cm^{-1} band dominates the spectrum at high concentrations of t-$BuNH_2$, leaving the band at 1645 cm^{-1} as a shoulder.

Acknowledgments

The authors are indebted to the New Zealand government for the award of a Commonwealth Scholarship to Pius Kipkemboi, and to the University of Auckland Research Committee for equipment funding.

References

1. S. Singh and P.J. Krueger. J. Raman Spectrosc. **13**, 178 (1982).
2. Zh.S. Nickolov, J.C. Earnshaw, J.J. McGarvey, and G.M. Georgiev. J. Raman Spectrosc. **25**, 837 (1994).
3. W.B. Fischer, H.H. Eysel, O.F. Nelsen, and J.E. Bertie. Appl. Spectosc. **48**, 107 (1994).
4. D. Jamroz, J. Stangret, and J. Lindgren. J. Am. Chem. Soc. **115**, 6165 (1993).
5. J.L. Green, A.R. Lacey, and M.G. Sceats. Chem. Phys. Lett. **137**, 537 (1987).
6. C.H. Spink and J.C. Wyckoff. J. Phys. Chem. **76**, 1660 (1972).
7. R.T. Yang and M.J. Low. Spectrochim. Acta, **30A**, 1787 (1974).
8. O.D. Bonner and Y.S. Choi. J. Sol. Chem. **4**, 457 (1975).
9. K. Tanabe and S. Tsuzuki. Spectrochim. Acta, **42A**, 611 (1986).
10. I. Auzanneau, D. Combes, and A. Zwick. J. Raman Spectrosc. **22**, 227 (1991).
11. H.J. Himmler and H.H. Eysel. Spectrochim. Acta, **45A**, 1077 (1989).
12. M. Moskovitis and K.H. Michaaelian. J. Am. Chem. Soc. **102**, 2209 (1980).
13. P.K. Kipkemboi and A.J. Easteal. Can. J. Chem. **72**, 1937 (1994).
14. P.K. Kipkemboi and A.J. Easteal. Aust. J. Chem. **47**, 1771 (1994).
15. P.K. Kipkemboi and A.J. Easteal. Bull. Chem. Soc. Jpn. **67**, 2956 (1994).
16. P.K. Kipkemboi and L.A. Woolf. J. Chem. Eng. Data, **40,** 943 (1995).
17. P.K. Kipkemboi and A.J. Easteal. J. Kenya Chem. Soc. **1**, 20 (1999).
18. P.A. Giguére and M. Pigeon-Gosselin. J. Raman Spectrosc. **17**, 341 (1986).
19. F. Rull and J.A. de Saja. J. Raman Spectrosc. **17**, 167 (1986).